J. Fluid Mech. (1997), *vol.* 334, *pp.* 61–86

The evolution of a uniformly sheared thermally stratified turbulent flow

By PAUL PICCIRILLO† AND CHARLES W. VAN ATTA‡

Department of Applied Mechanics and Engineering Sciences, University of California, San Diego, La Jolla, CA 92093, USA

(Received 10 October 1994 and in revised form 26 September 1996)

Experiments were carried out in a new type of stratified flow facility to study the evolution of turbulence in a mean flow possessing both uniform stable stratification and uniform mean shear.

The new facility is a thermally stratified wind tunnel consisting of ten independent supply layers, each with its own blower and heaters, and is capable of producing arbitrary temperature and velocity profiles in the test section. In the experiments, four different sized turbulence-generating grids were used to study the effect of different initial conditions. All three components of the velocity were measured, along with the temperature. Root-mean-square quantities and correlations were measured, along with their corresponding power and cross-spectra.

As the gradient Richardson number $Ri = N^2/(\mathrm{d}U/\mathrm{d}z)^2$ was increased, the downstream spatial evolution of the turbulent kinetic energy changed from increasing, to stationary, to decreasing. The stationary value of the Richardson number, Ri_{cr}, was found to be an increasing function of the dimensionless shear parameter Sq^2/ϵ (where $S = \mathrm{d}U/\mathrm{d}z$ is the mean velocity shear, q^2 is the turbulent kinetic energy, and ϵ is the viscous dissipation).

The turbulence was found to be highly anisotropic, both at the small scales and at the large scales, and anisotropy was found to increase with increasing Ri. The evolution of the velocity power spectra for $Ri \leqslant Ri_{cr}$, in which the energy of the large scales increases while the energy in the small scales decreases, suggests that the small-scale anisotropy is caused, or at least amplified, by buoyancy forces which reduce the amount of spectral energy transfer from large to small scales. For the largest values of Ri, countergradient buoyancy flux occurred for the small scales of the turbulence, an effect noted earlier in the numerical results of Holt *et al.* (1992), Gerz *et al.* (1989), and Gerz & Schumann (1991).

1. Introduction

Stable stratification is a ubiquitous feature of turbulent shear flows in nature and in technological applications. Geophysical examples include flow in the ocean thermocline (Gregg 1987), or in capping inversions in the atmosphere (Singh Khalsa & Greenhut 1987). Engineering applications include dispersal of waste pollutants into stratified coastal waters or into the atmosphere. The physics of turbulent mixing in such flows can be usefully studied by considering the simplified case of a developing laterally

† Present address: Department of Civil Engineering, Stanford University, Stanford, CA 94305-4020, USA.

‡ Also Scripps Institution of Oceanography, La Jolla, CA 92093, USA.

homogeneous turbulent shear flow with constant gradients of mean velocity and density. In the present study, we experimentally examine such a flow, to determine how the evolution and structure of the turbulence, and the resultant fluxes of buoyancy and momentum, are affected by the presence of stable stratification.

Owing to insufficient test section length, early experimental work studying turbulent evolution in purely sheared flows, such as that of Rose (1966, 1970) or Champagne, Harris & Corrsin (1970) found the turbulent kinetic energy to approach a constant level downstream of a generating grid. Later work by Harris, Graham & Corrsin (1977), Rohr *et al.* (1988*a*), and Tavoularis & Karnik (1989) established clearly that, with sufficient test section length and with a sufficient amount of shear, the turbulent kinetic energy will grow downstream of a generating grid. The experiments of Tavoularis & Corrsin (1981*a*, *b*) and Budwig, Tavoularis & Corrsin (1985) showed that this behaviour also exists in the case of passive stratification. Computational work, such as that by Rogallo (1981), Feiereisen *et al.* (1982), Rogallo & Moin (1984), and Rogers, Moin & Reynolds (1986), who also added passive scalars, show good agreement with the experimental results, and present much information on aspects of the turbulent evolution not easily investigated in the laboratory, such as the existence of large-scale coherent vortex structures caused by the interaction of the mean shear with the turbulence.

The effects of a stable density stratification on the evolution of turbulence have been thoroughly investigated for a uniform mean flow. Experiments using salt stratification in water by Stillinger, Helland & Van Atta (1983), Itsweire, Helland & Van Atta (1986), Barrett & Van Atta (1989), Yap & Van Atta (1993), Liu (1995), and Fincham, Maxworthy & Spedding (1997), and experiments using temperature stratification in air by Lienhard & Van Atta (1990), Yoon & Warhaft (1990), and Thoroddsen & Van Atta (1992, 1996) have shown conclusively that the buoyancy forces created by the stable stratification strongly suppress the vertical component of the turbulent kinetic energy. Also, the buoyancy flux in the flow, initially downgradient due to turbulent mixing, becomes countergradient at the largest scales of the turbulence, as fluid parcels begin to move back to their equilibrium positions in the flow. Thoroddsen & Van Atta (1996) found that stratification also produced an unexpected rapid onset of anisotropy in the small scales of their decaying turbulence. Complementary results, consistent with the experimental findings, have been obtained in many numerical simulations, including those of Riley, Metcalfe & Weissman (1981), and Herring & Metais (1989).

Experiments combining uniform mean shear and stable stratification were carried out in salt-stratified water by Rohr *et al.* (1988*b*). They found that at a critical value Ri_{cr} of the gradient Richardson number $Ri = N^2/(\mathrm{d}U/\mathrm{d}z)^2$ ($N = [(g/T_0)(\mathrm{d}T/\mathrm{d}z)]^{1/2}$ is the Brunt–Väisälä frequency) of 0.25 ± 0.05, the turbulent kinetic energy of the flow became independent of the development distance x, the coordinate in the mean flow direction. They also found that the primary means by which buoyancy affected the turbulence was by reducing turbulent production, inferred to be associated with buoyancy suppression of the spatial coherence of the large eddies in the flow.

Numerical simulations carried out by Gerz, Schumann & Elghobashi (1989), Gerz & Schumann (1991), Schumann & Gerz (1995), and Kaltenbach, Gerz & Schumann (1994) suggest that the critical value of Ri can be lower than the 0.25 ± 0.05 given by Rohr *et al.* (1988*b*). They found the velocity strain rates to be less anisotropic than the r.m.s. velocity fluctuations. They found countergradient velocity density fluxes, which were not seen by Rohr *et al.* (1988*b*), but only for large Ri (greater than 0.33) and high Prandtl number. These density fluxes occurred primarily at small scales, unlike those in the unsheared experiments of Lienhard & Van Atta (1990), Yoon & Warhaft (1990),

and Thoroddsen & Van Atta (1992, 1996), where the countergradient heat fluxes were produced by large-scale transport. Also, Gerz & Schumann (1991) found both the velocity and temperature dissipation to be greater than in the unsheared case. They attributed this to shear-induced gravity wave breaking, as suggested by Hunt, Stretch & Britter (1988), and found experimentally by Britter (1988).

Another set of simulations was carried out by Holt, Koseff & Ferziger (1992), and extended by Ivey *et al.* (1992) and Itsweire *et al.* (1993). In them, the critical *Ri* was found to be an increasing function of the initial turbulence Reynolds number $Re_{\Lambda i} = \mu'\Lambda/\nu$, where Λ is the integral scale of the turbulence. The velocity strain rates were found to be more anisotropic than the velocity r.m.s. fluctuations, and countergradient heat fluxes were found at large *Ri*, again primarily at small scales. The anisotropy of r.m.s. velocity fluctuations was found to be at a maximum at the *Ri* where the net vertical density flux changed sign. The subsequent net countergradient flux then reduced the amount of anisotropy, a result consistent with those of Gerz *et al.* (1989). Finally, Holt *et al.* found that at Ri_{cr}, the one-dimensional velocity spectra were not constant, as the large scales were gaining energy while the small scales were losing energy, consistent with the results of Rohr *et al.* (1988*b*). Recent simulations carried out by Jacobitz, Sarkar & Van Atta (1994, 1996) found Ri_{cr} to be a strong function of the dimensionless shear parameter Sq^2/ϵ (where $S = \mathrm{d}U/\mathrm{d}z$ is the mean velocity shear, q^2 is the turbulent kinetic energy, and ϵ is the viscous dissipation) as well as a function of the initial Reynolds number $R_\lambda = q\lambda/\nu$. Here, $\lambda = (5q^2\nu/\epsilon)^{1/2}$ is the Taylor microscale.

The present facility and experiments were largely motivated by the desire to obtain better data than was possible in the water tunnel of Rohr *et al.* (1988*b*), for a substantially different ratio of viscous to scalar diffusivity (the Prandtl number for air is 0.7, while the Schmidt number for salt-stratified water is around 700). Comparing the numerical simulations with the experiments raised several questions, suggesting interesting new avenues for experimentation. These included determining (*a*) the dependence of Ri_{cr} on the shear parameter Sq^2/ϵ and Re_Λ, (*b*) the effect of the buoyancy on the anisotropy of the large and small scales of the turbulence, and (*c*) whether the small-scale countergradient cospectral buoyancy flux and the countergradient Reynolds stress results found in the simulations would occur in a physical experiment. We did not realize the importance of the shear parameter Sq^2/ϵ, despite its prominence in the non-stratified case, until after the present experiments were completed. As the DNS results of Jacobitz *et al.* (1995) became available during the preparation of this paper, interpretation of the experimental results was greatly enhanced by insights from these DNS.

Because of the well-resolved results achieved by Lienhard & Van Atta (1990) and Thoroddsen & Van Atta (1992, 1996), it was decided to use thermally stratified air as the medium in which to conduct our experiments. We note that such an approach was also adopted by Webster (1964) in his pioneering experiments on a density-stratified shear flow. Owing to the unique requirements of the experiments to be performed, a new type of facility was designed and built. With this new facility, we have performed the first experiments in air which have both velocity shear and strong thermal stratification, and for which the development distance is sufficiently long to observe growing, decaying, or constant levels of turbulent kinetic energy.

In the remainder of this section, we will discuss the equations of motion of our study. In §2, the experimental procedure will be outlined. In §3, we examine the second-order moments of the turbulence, with our primary focus being on the factors influencing the critical value of *Ri*. In §4, we discuss the anisotropy of the flow. In §5, we present the

spectral and cospectral behaviour of the turbulence, and in §6, we will discuss our results and attempt to draw some overall conclusions.

1.1. *The equations of motion*

We assume that the mean flow is incompressible and transversely homogeneous. We also assume that the Boussinesq approximation is valid in this case, allowing us to remove the fluctuating fluid density from the inertia terms in the equations. Finally, we assume that the triple-correlation divergence terms are negligibly small, as found experimentally for the unsheared case by Lienhard (1988). The resulting equations for each component of the turbulent kinetic energy are

$$U\frac{\partial\overline{\frac{1}{2}u^2}}{\partial x} = -\overline{uw}\frac{\mathrm{d}U}{\mathrm{d}z} + \frac{1}{\rho_0}\overline{p\frac{\partial u}{\partial x}} - \nu\overline{\left(\frac{\partial u}{\partial x_k}\right)^2}, \tag{1}$$

$$U\frac{\partial\overline{\frac{1}{2}v^2}}{\partial x} = \frac{1}{\rho_0}\overline{p\frac{\partial v}{\partial y}} - \nu\overline{\left(\frac{\partial v}{\partial x_k}\right)^2}, \tag{2}$$

$$U\frac{\partial\overline{\frac{1}{2}w^2}}{\partial x} = \overline{w\theta}\frac{g}{T_0} + \frac{1}{\rho_0}\overline{p\frac{\partial w}{\partial z}} - \nu\overline{\left(\frac{\partial w}{\partial x_k}\right)^2}, \tag{3}$$

where u, v, and w are the streamwise, lateral, and vertical fluctuating velocity components, respectively, and the overbar denotes time averaging. Summing these equations, we arrive at the turbulent kinetic energy evolution equation for sheared, buoyancy-affected turbulence:

$$U\frac{\partial\overline{\frac{1}{2}q^2}}{\partial x} = -\overline{uw}\frac{\mathrm{d}U}{\mathrm{d}z} + \overline{w\theta}\frac{g}{T_0} - \epsilon. \tag{4}$$

In this equation $\epsilon = \nu\overline{(\partial u_i/\partial x_k)(\partial u_i/\partial x_k)}$ is the viscous dissipation. It should also be noted that we have changed the density term $(g_i/\rho_0)\,\overline{u_i\rho}$ into a temperature term using the perfect gas equation, since our stratifying agent will be temperature.

In (4), the turbulent kinetic energy has one direct source term, the production term, and two sink terms, the buoyancy term and the viscous dissipation. Thus, in order for the turbulence to grow downstream, the source term must be larger than the buoyancy term and the dissipation together. This suggests that small changes in the value of the $\overline{uw}$ correlation will have a large effect on the behaviour of the turbulent kinetic energy. The anisotropic nature of the source and sink terms can be clearly seen in (1), (2), and (3), where the production term occurs only in the equation for $\overline{u^2}$, while the buoyancy term occurs only in the $\overline{w^2}$ equation.

The evolution of the scalar variance is given by

$$U\frac{\partial\overline{\frac{1}{2}\theta^2}}{\partial x} = -\overline{w\theta}\frac{\mathrm{d}T}{\mathrm{d}z} - \chi. \tag{5}$$

Here, $\chi = \alpha\overline{(\partial\theta/\partial x_j)(\partial\theta/\partial x_j)}$ is the scalar dissipation. For downgradient turbulent mixing, the buoyancy flux term is a sink of kinetic energy and a source of scalar variance.

2. Experimental procedure

The experiments were performed in a new type of thermally stratified wind tunnel, shown in figure 1. It consists of ten separate horizontal layers, each with its own blower and electrical heater assembly, and is capable of producing flows with N up to

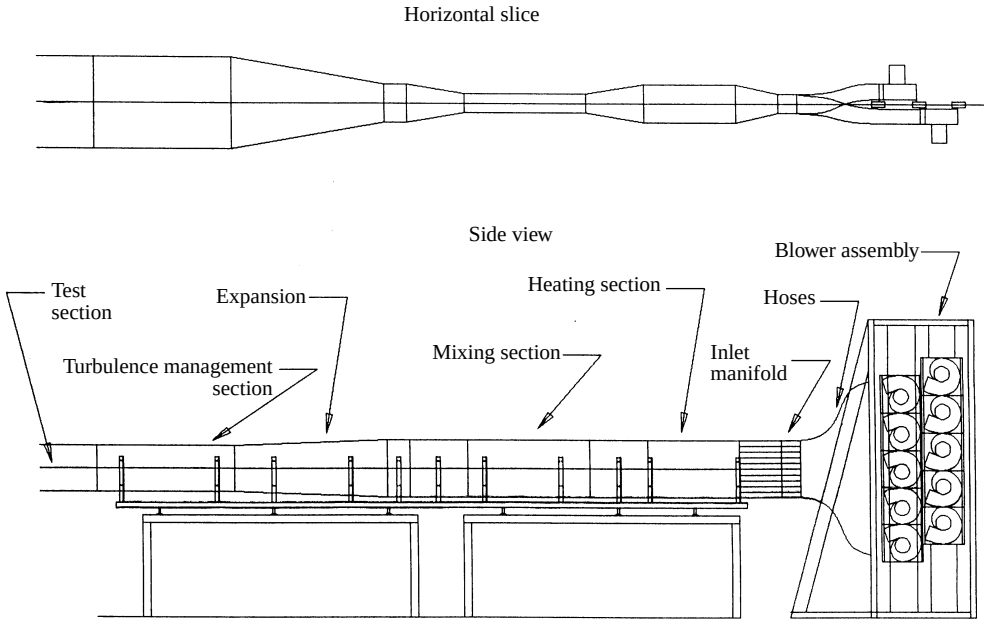

FIGURE 1. Sketch of the stratified-shear-flow wind tunnel (hose detail not shown for clarity).

Run number	*Ri*	Shear (s^{-1})	*N* (rad s^{-1})
1	0	4.45	0
2	0.04	4.45	0.91
3	0.08	4.45	1.24
4	0.12	4.45	1.55
5	0.19	4.45	1.98
6	0.44	3.35	2.23

TABLE 1. Experimental runs

2.5 rad s^{-1} and mean velocity shears (dU/dz) of up to 5 s^{-1} at a nominal mean velocity of 2 m s^{-1}. The mean vertical velocity and temperature profiles generated by the tunnel were found to depart from linearity by no more than 0.5 °C and 3 cm s^{-1}. Also, turbulence generated in the tunnel was found to be transversely and vertically homogeneous to within about 15%. For more details concerning the design of the tunnel and performance, see Piccirillo (1993) and Piccirillo & Van Atta (1996).

The main parameters varied in our study were the Richardson number *Ri* and the shear parameter Sq^2/ϵ. Tunnel operating limitations precluded a significant variation in Reynolds number. The turbulence was generated by one of four biplanar grids, with grid mesh spacings of 5.08, 2.54, 1.45 and 0.64 cm, with constant solidity. The differing grid sizes created differing values of Sq^2/ϵ and $Re_{\Lambda i}$, the initial Reynolds number of the turbulence. The test section in which the turbulence evolved is 5.49 m long, with a cross-section that is initially 30.5 cm high by 61 cm wide. The top and bottom walls of the test section are adjusted for boundary layer growth so that the mean velocity at the centreline of the test section remains nearly constant throughout its length.

Data were taken using the cross-wire/cold-wire technique developed by Lienhard (1988) and Lienhard & Van Atta (1990). Both *uw*-measurements, where the vertical

velocity is measured, and *uv*-measurements, where the lateral velocity is measured, were performed. For each run, nineteen downstream measuring stations were used for *uw*-measurements, with seven of these also used for *uv*-measurements. All of the runs described here were performed with the probe on the centreline of the test section.

The values of $S = \mathrm{d}U/\mathrm{d}z$, N, and Ri for the different Ri runs are given in table 1. The mean centreline velocity in all of the runs was approximately 1.90 m s^{-1}, except for $Ri = 0.44$, where the mean velocity was approximately 2.20 m s^{-1}. This difference in velocity had no noticeable effect on the behaviour of the turbulence for any of the mesh sizes used. Also, in the $Ri = 0.44$ runs, the mean velocity shear was smaller than in the other runs.

In this paper we can present only a small amount of the experimental results. Tables providing results for all of the experiments have been archived with the *Journal of Fluid Mechanics*, and are available upon request from the Editorial Office. Many additional figures can be found in Piccirillo (1993). Information on some mislabelling which occurred in these thesis figures is provided along with the tables, which are correctly labelled.

To compute the turbulent kinetic energy at stations where *uv*-measurements were not taken, v'/w' was calculated for the points where *uv*- and *uw*-measurements were taken, where the primes signify the r.m.s. values of the fluctuations (which are equal to the square roots of the variances of these quantities); v'/w' was then estimated for the remaining points by interpolation, and the resulting estimate for v' then calculated from w'. This estimate, v'_e was then used to calculate q. In order to estimate a value for the critical Ri, Ri_{cr}, the q-data were examined, for each Ri, from 3 m downstream of the generating grid to the end of the test section. If the data were constant to within 2%, that Ri was chosen as Ri_{cr}.

The dissipation was estimated using the three measured strain rates via the formula (Piccirillo 1993)

$$\epsilon = \nu\left[5\overline{\left(\frac{\partial u}{\partial x}\right)^2} + \frac{5}{2}\overline{\left(\frac{\partial v}{\partial x}\right)^2} + \frac{5}{2}\overline{\left(\frac{\partial w}{\partial x}\right)^2}\right]. \tag{6}$$

For locations where the lateral velocity strain rate was not measured, it was estimated using an interpolation scheme identical to the one used for estimating the lateral velocity fluctuations discussed above.

3. Behaviour of second-order single-point moments

3.1. *Turbulent velocity and temperature moments*

The evolution of $q/U = (u^2+v^2+w^2)^{1/2}/U$ versus downstream position as a function of Ri is shown for the 1.45 cm grid in figure 2. As has been seen by previous researchers, as Ri increases, q changes behaviour, from strongly increasing at $Ri = 0$ to decreasing at $Ri = 0.44$. At $Ri = 0$, q grows in the exponential manner seen by Rohr *et al.* (1988*a*). For $Ri = 0.44$, the decay of q is slower than in the case of unforced, initially isotropic turbulence, suggesting that the mean shear is still strongly influencing the evolution of the turbulence.

The behaviour of the individual components of q is very similar to that of q. The only important difference between the three components is the location of their minimum value in the cases where they subsequently increase. The minima for u', w', and v' are at $\tau = (x/U)(\mathrm{d}U/\mathrm{d}z)$ of 2.9–3.5, 4.6 and 3.5 respectively. The slower evolution of w' is due to buoyancy forces influencing the pressure redistribution of the velocity

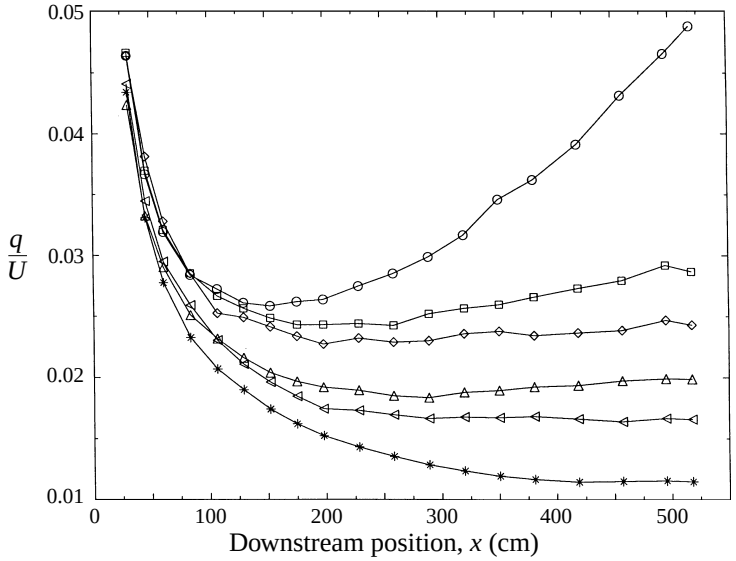

FIGURE 2. Evolution of q/U for all Ri, 1.45 cm grid. Symbols: ○---○, $Ri = 0$; □---□, $Ri = 0.04$; ◇---◇, $Ri = 0.08$; △---△, $Ri = 0.12$; ◁---◁, $Ri = 0.19$, ∗---∗, Ri = 0.44.

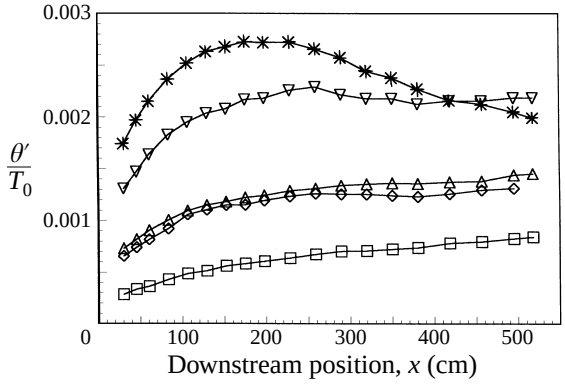

FIGURE 3. Evolution of θ'/T_0 for all Ri, 1.45 cm grid. Symbols same as in figure 2.

fluctuations. For u' and w', Rohr *et al.* (1988*b*) obtain minima at τ of 2 and 3 respectively, while Holt *et al.* (1992) obtain values of 2 and 3.5–4.0 and Gerz *et al.* (1989) obtain values of less than 0.5 and 3.5. This is reasonably good agreement, especially considering the differences in initial conditions between the experiments and the simulations.

The evolution of θ'/T_0, the normalized r.m.s. temperature, is plotted in figure 3. It is clear that the behaviour of the r.m.s. temperature is closely linked to that of q. When q is increasing downstream, θ' also increases downstream. When q becomes stationary, θ' increases initially and levels off at between 300 and 400 cm downstream ($\tau = 7$–9). This location is an increasing function of decreasing grid mesh size. When q is decreasing, θ' increases initially to a maximum at a downstream position of about 200 cm ($\tau = 4.5$), and then decays throughout the remainder of the test section. Rohr (1985) finds the density fluctuations to decrease for $\tau > 6$ in all cases, while Holt *et al.*

Ri_{cr}	Grid mesh size (cm)	$(Re_\Lambda)_i$	$(Sq^2/\epsilon)_i$	Re_Λ	Sq^2/ϵ
Present results					
0.04	5.08	32.5	0.30	190.2	7.75
0.08	2.54	24.0	0.38	146.8	9.75
0.19	1.45	15.1	0.42	142.9	22.45
0.19	0.64	13.2	0.62	131.7	35.80
Holt *et al.* results					
0.0575	—	25.8	5.74	69.4	12.22
0.0875	—	51.7	5.74	115.6	11.00
0.1125	—	103.5	5.74	139.7	11.55
0.15	—	104.0	5.78	291.4	10.81
0.21	—	80.1	2.74	343.3	10.66

TABLE 2. Ri_{cr} as a function of $(Re_\Lambda)_i$ and $(Sq^2/\epsilon)_i$, and Re_Λ and Sq^2/ϵ for $\tau > 10$, where i denotes initial.

(1992) and Gerz *et al.* (1989) find results qualitatively identical to ours. Quantitatively, both of the simulations report τ-values of between 2 and 4 for the region in which the density fluctuations change behaviour.

3.2. *Dependence of Ri_{cr} on shear parameter and Reynolds number*

Using the Ri_{cr} criterion that the turbulent kinetic energy become independent of downstream coordinate x, as discussed in §2, Ri_{cr} was estimated from the runs for each of the four different mesh size grids. The results are given in table 2, along with the results of the numerical simulations of Holt *et al.* (1992). Uncertainties in comparing the experimental and DNS results arise from the very different initial conditions in the two cases. For example, the Holt *et al.* (1992) DNS used an initial 'top-hat' velocity energy spectrum which differs greatly from the initial experimental spectrum. One hopes that comparison of the two cases becomes more rigorous for long time evolutions in the DNS and far downstream locations in the experiments. With this in mind, we compare in table 2 the initial values of Re_Λ and Sq^2/ϵ, as well as values calculated far downstream ($\tau > 10$). Here, $Re_\Lambda = q\Lambda/\nu$, where $\Lambda = u'^3/\epsilon$. This definition differs slightly from that used by Holt *et al.*

For our data, Ri_{cr} increases from 0.04 to 0.12–0.19 as the initial value of Sq^2/ϵ increases by a factor of 2 and the corresponding Re_Λ decreases by a factor of 2.5. If the initial values of Sq^2/ϵ and Re_Λ had been varied independently in the experiments, then we could conclude that the increase in Ri_{cr} with increasing Sq^2/ϵ agrees with the behaviour of the Jacobitz *et al.* (1996) simulations, while the decrease of Ri_{cr} with increasing Re_Λ disagrees with these simulations and those of Holt *et al.* (1992). But, as explained above, the initial values of the two parameters could not be varied independently in the experiments. We therefore pursue the alternative of comparing results for large DNS evolution times with experimental results obtained further downstream, after the shear and buoyancy have had a strong effect on the flow evolution.

As seen in table 2, making this comparison for large values of τ, the increase in Ri_{cr} is accompanied by an increase of 4.6 Sq^2/ϵ as Re_Λ decreases by only 30%, so that the variation in Re_Λ is an order of magnitude smaller than that in Sq^2/ϵ. Ignoring the possible effects of the relatively small change in Re_Λ, and giving precedence to the data for large τ over the initial data, our experiments show that Ri_{cr} is an increasing function of Sq^2/ϵ. One way to rationalize this result is to note that, by scaling the terms in equation (4), Sq^2/ϵ is proportional to the ratio of the turbulence production and

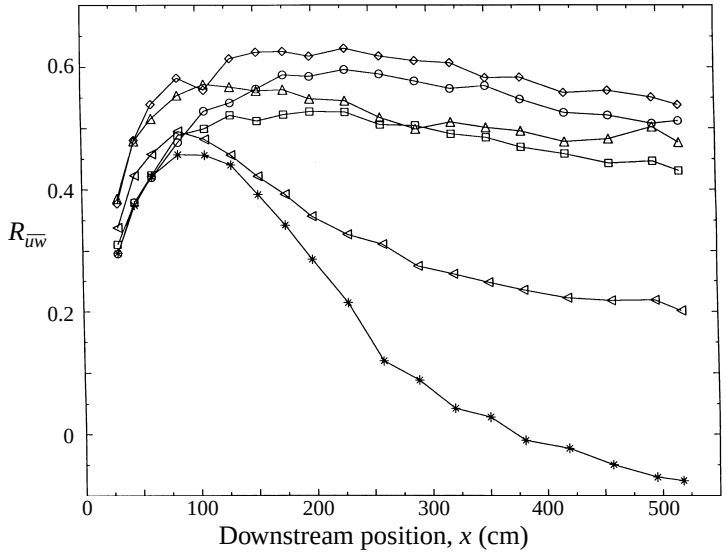

FIGURE 4. Evolution of $R_{\overline{uw}}$ for all Ri, 1.45 cm grid. Symbols same as in figure 2.

dissipation terms. As Sq^2/ϵ increases, the relative value of the dissipation decreases, and with less dissipation, the stratification necessary to change the behaviour of q will increase. Thus we would expect that Ri_{cr} will be an increasing function of Sq^2/ϵ. Indeed, recent simulations of the present flow by Jacobitz *et al.* (1996) show that Ri_{cr} is an increasing function of Sq^2/ϵ for small initial values of Sq^2/ϵ covering the present range of 0.3 to 0.6. In the simulations, for a fixed initial value of Ri_{cr}, as Sq^2/ϵ is further increased, Ri_{cr} reaches a maximum and then decreases for large values of Sq^2/ϵ, as would be expected from the rapid-distortion analysis of Hunt *et al.* (1988).

Rohr *et al.* found $Ri_{cr} = 0.25 \pm 0.05$, which is consistent with the trend of our data in view of their large values of Sq^2/ϵ of 20 for $\tau = 10$, and Re_Λ of greater than 200. Gerz *et al.* obtain a value of about 0.10 for their simulation, which was for Re_Λ of 47.2. Neither Rohr *et al.* nor Gerz *et al.* examined the behaviour of Ri_{cr} with Sq^2/ϵ. Holt *et al.* (1990) performed some simulations in which Sq^2/ϵ was increased to 50 and 100. Although the results of these runs are not definitive, increasing Sq^2/ϵ apparently increased the value of Ri_{cr} in these simulations, in agreement with our results. Our data show an apparent decrease in Ri_{cr} with an increasing Re_Λ, but this trend may not be significant in view of the small range of variation of R_Λ and the simultaneous much larger changes in Sq^2/ϵ, whose influence may dominate that of Re_Λ. This conjecture appears to be supported by the results of Holt *et al.* as shown in table 2. For nearly constant Sq^2/ϵ they found that an increase of Ri_{cr} over the range we observed required a fivefold increase in Re_Λ.

There are many other factors which could affect the value of Ri_{cr}. These include $N\theta^2/\chi$, the scalar analogue of the dimensionless shear, the ratio of fluctuating potential energy $\frac{1}{2}g\theta^2/\Theta(\mathrm{d}\Theta/\mathrm{d}z)$ to the turbulent kinetic energy, as well as the Prandtl or Schmidt number of the flow. The effect of Pr or Sc seems especially significant, as Rohr *et al.* and Holt *et al.* find that larger values of Pr or Sc lead to lower correlations for the velocity and the density, which may then lead to higher values of Ri_{cr} (for example, Rohr *et al.*'s value of 0.25).

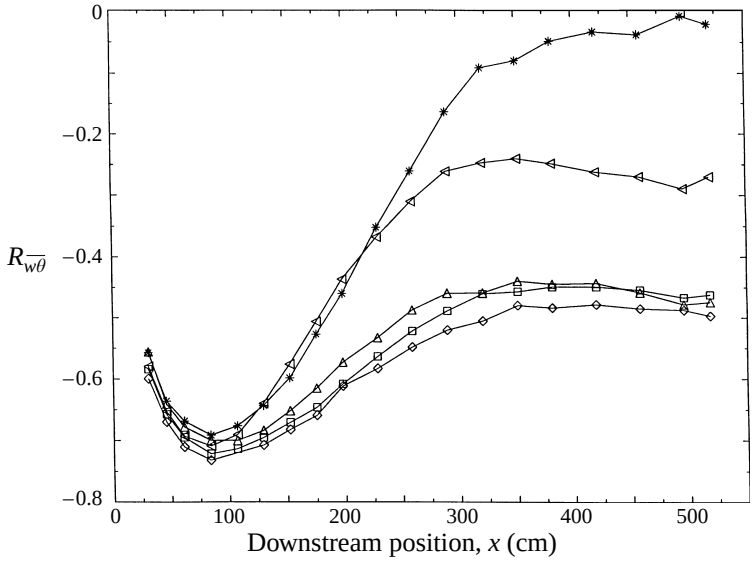

FIGURE 5. Evolution of $R_{\overline{w\theta}}$ for all $Ri > 0$, 1.45 cm grid. Symbols same as in figure 2.

3.3. *Momentum and heat-flux correlations*

The evolution of the Reynolds stress correlation coefficient, $R_{\overline{uw}} = \overline{uw}/u'w'$, is shown for the 1.45 cm grid in figure 4. For the unstratified case, $R_{\overline{uw}}$ quickly reaches a maximum of around 0.55–0.60, somewhat higher than the value of 0.48 found by Tavoularis & Karnik (1989). The addition of stratification produces a small decrease in value for $R_{\overline{uw}}$ until the $Ri = 0.19$ case, for which the value for $R_{\overline{uw}}$ dramatically decreases downstream of the maximum. For the $Ri = 0.44$ case, $R_{\overline{uw}}$ was, for all the grids, less than 0.10. The evolution of $R_{\overline{uw}}$ was the same for all of the grids. Similar variations of Reynolds stress (and vertical heat transfer) with Ri were observed in wind tunnel experiments by Webster (1964) and Komori *et al.* (1983) in a stably stratified open channel flow. The present results also agree well with the results of both Rohr *et al.* (1988*b*), and Holt *et al.* (1992), who find $R_{\overline{uw}}$ to be slowly decreasing with Ri for $Ri < 0.25$, and then dramatically decreasing for $Ri \geqslant 0.25$, while Gerz *et al.* (1989) find a more even decrease of $R_{\overline{uw}}$ with Ri. Quantitatively, our final values for $R_{\overline{uw}}$ are about 20% higher than those of Rohr *et al.* and Holt *et al.* for similar Ri.

The evolution of the buoyancy-flux correlation coefficient $R_{\overline{w\theta}} = \overline{w\theta}/w'\theta'$ is shown in figure 5. The behaviour is similar to that seen for the Reynolds stress correlation. For all of the grids, $R_{\overline{w\theta}}$ decreases as Ri is increased. However, for no run in these experiments was a net flux reversal (i.e. $\overline{w\theta} > 0$) observed. The maximum value of $R_{\overline{w\theta}}$ reached in our experimental results was -0.75, a very high value reached rarely in unsheared experiments. The values obtained by Rohr (1985) were considerably lower, perhaps due to the higher Schmidt number of his flow. Rohr also did not observe a buoyancy-flux sign reversal. Holt *et al.* did not find any such flux reversal until $Ri >$ 0.50. Quantitatively, the simulation had a much higher maximum value for $R_{\overline{w\theta}}$, higher in fact than any value reported in an experimental study, including the non-sheared results of Lienhard & Van Atta (1990), Thoroddsen (1991), and Yoon & Warhaft (1990). This differs from the Reynolds stress behaviour, where the maximum reached by $R_{\overline{uw}}$ was greater in the experiment than in the simulation. The Gerz *et al.* simulation reported flux reversals for Ri as low as 0.3, disagreeing with our experiments, Rohr's experiments, and Holt *et al.*'s simulation.

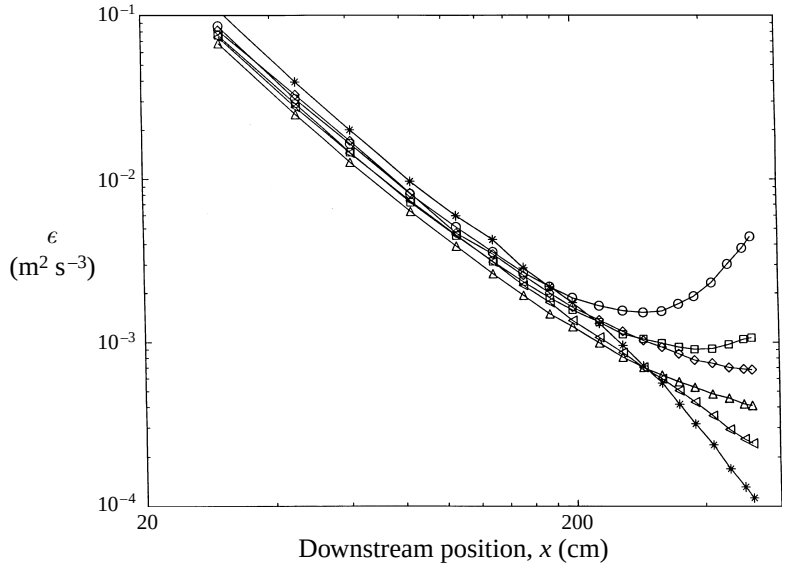

FIGURE 6. Evolution of ϵ, the viscous dissipation, for all Ri, 1.45 cm grid. Symbols same as in figure 2.

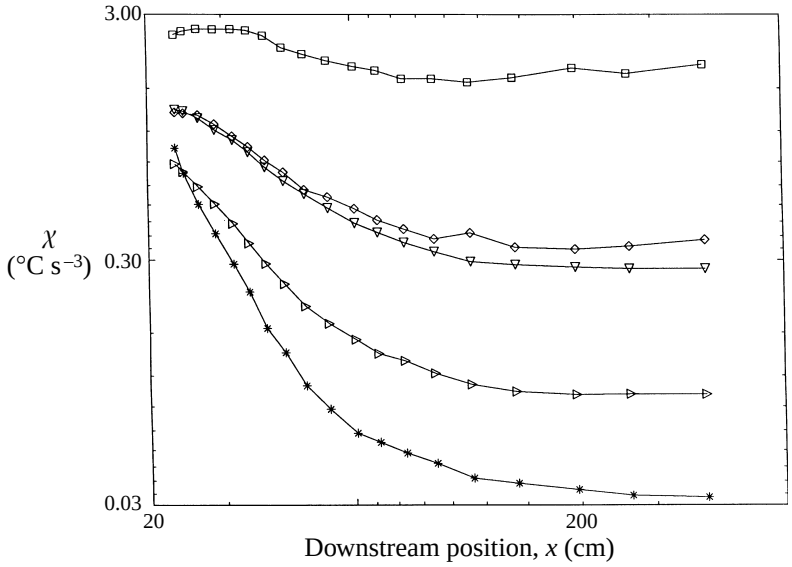

FIGURE 7. Evolution of χ, the scalar dissipation, for all $Ri > 0$, 1.45 cm grid. Symbols same as in figure 2.

We have seen that the addition of stable stratification to a uniform-mean-shear turbulent flow reduces the value of both the buoyancy flux and the Reynolds stress in the flow. The reduction of the Reynolds stress is the result of buoyancy forces breaking the large coherent structures that result from the interaction of the turbulence and the mean shear, while the reduction in $R_{\overline{w\theta}}$ is the result of the buoyancy attempting to restratify the fluid.

3.4. *Dissipation*

The results of the dissipation-rate estimation calculations are shown in figure 6 for the 1.45 cm grid. For $\tau < 7$, the dissipation is roughly independent of Ri. For $\tau > 7$, the dissipation becomes a strongly decreasing function of Ri, with there being approximately an order of magnitude difference between the $Ri = 0$ and $Ri = 0.44$ dissipation estimates by the end of the test section ($\tau = 12$). The individual strain rates which combine to form our dissipation estimate behave qualitatively identically to their sum. The difference in the final values of q between the $Ri = 0$ and the $Ri = 0.44$ cases is a factor of 3, which is considerably smaller than the difference in the final values of ϵ. This suggests that buoyancy forces influence dissipation more strongly than they do turbulent kinetic energy.

Our results compare well with those of Rohr (1985) for $\tau > 7$, showing the same general evolution pattern and the same one order of magnitude spread in ϵ at $\tau = 12$. For $\tau < 7$, Rohr's data are clearly a decreasing function of Ri, whereas ours are not. Holt (1990), who 'tuned' his code to match Rohr's results, presents results qualitatively similar to those of Rohr.

The evolution of the rate of scalar dissipation is shown for the 1.45 cm grid in figure 7. The dissipation was estimated using the isotropic formula:

$$\chi = 6\alpha\overline{\left(\frac{\partial\theta}{\partial x}\right)^2}. \tag{7}$$

Using the isotropic formula in this case will lead to errors in estimating the value of χ, as discussed in Thoroddsen & Van Atta (1993), but the difficulties involved in getting accurate strain rate estimations for the non-streamwise directions forces us to use the isotropic formula. The results are similar for all of the grid configurations, differing only in magnitude. For all of the grids and all Ri, χ started as a near constant, and then gradually decreased, with the rate of decay increasing until the end of the test section, in most cases. In some low-Ri cases where θ' was increasing throughout the test section, the dissipation increased for large τ.

Unfortunately, owing to the small diffusivity of salt in water, as discussed in §1, Rohr (1985) was unable to estimate his scalar dissipation. Our results are thus the first experimental estimation of the scalar dissipation in a uniform-velocity-shear stably stratified flow to date. The χ results of Holt (1990) are difficult to compare with our results, as his initial conditions include having $\theta'(\tau = 9) = 0$. The results of Gerz *et al.* do not agree with ours, as they find χ increasing everywhere for $Ri < Ri_{cr}$. This behaviour differs from the unsheared results of Thoroddsen (1991) and Lienhard & Van Atta (1990), for which there is no region of nearly constant χ.

3.5. *Mixing efficiency*

A quantity of great interest to oceanographers in the mixing efficiency or flux Richardson number, defined by Ivey & Imberger (1991) as

$$R_f = \frac{1}{1+(\epsilon/B)}, \tag{8}$$

where B is the buoyancy term in the turbulent kinetic equation (4). Ivey & Imberger (1991) found two semi-empirical curves for the behaviour of R_f as a function of the turbulent Froude number $Fr_T = (L_O/L_t)^{2/3}$, where $L_O = (\epsilon/N^3)^{1/2}$ is the Ozmidov scale, which estimates the largest scales not constrained by buoyancy, and $L_t = \theta'/(\mathrm{d}T/\mathrm{d}z)$

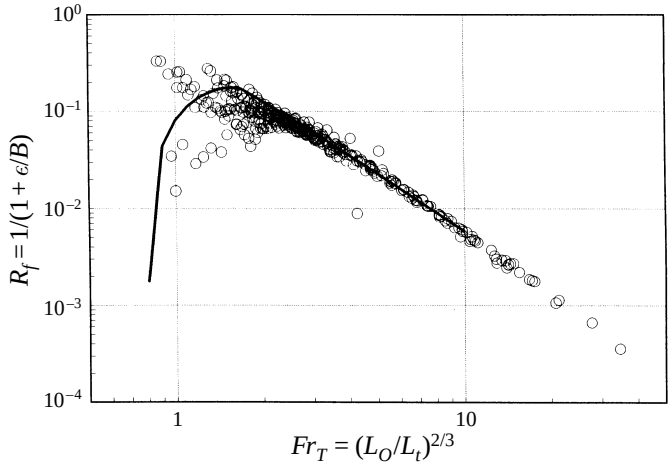

FIGURE 8. Evolution of the mixing efficiency, R_f as a function of the turbulent Froude number Fr_T. Open circles are data from the present experiments and the solid line the semi-empirical predictions of Ivey & Imberger (1991).

is the overturning scale of the turbulence. Our results are plotted with the Ivey & Imberger curve in figure 8. For $Fr_T > 2$, our data and the Ivey & Imberger curve agree very well. For $Fr_T < 2$, there is a lot of scatter in our data, which precludes any assessment of validity for the Ivey & Imberger curve at these values of Fr_T. The large amounts of scatter for $Fr_T < 2$ suggests that mixing in this region is dominated by powerful but rare mixing events. Also, our results show R_f values of up to 0.35, larger than seen in previous experiments. This is consistent with the idea of mixing dominated by rare events as, if these events are spaced randomly, a large number of them could lead to abnormally high values for R_f.

3.6. *Evolution of terms in the turbulent kinetic energy and temperature variance equations*

The evolution of the three terms on the right-hand side of equation (4) is plotted for $Ri < Ri_{cr}$ and $Ri = Ri_{cr}$ in figure 9. In both cases, the buoyancy term is very small compared to the production and dissipation terms, and is numerically (but not physically) unimportant in the turbulent kinetic energy balance of the turbulence. Looking at the production and the dissipation terms, when $Ri < Ri_{cr}$, as the flow develops downstream, the production, initially much smaller than the dissipation, eventually grows larger than it in magnitude. We then have production $> \epsilon$, which produces increasing q. In the case shown in the figure, we find that the growth rate for q predicted from a balance of the three terms matches the actual growth rate (averaged over the last 1.5 m of the test section) within 10%. In general, our agreement is not so good, being within 25%. When $Ri > Ri_{cr}$, the dissipation term remains larger than the production term throughout the test section, with the result that q decays. The predicted rates of decay from the three terms are accurate to within 30% of the actual decay of q, with the prediction being less than the actual value. This suggests that we have underestimated the dissipation in the flow, by amounts of up to 30%. Itsweire *et al.* (1993) suggest that using only the streamwise-direction strain rates, as we have done, could lead to underestimating the dissipation by up to a factor of 4. However, unlike our experiments, there was a large initial small-scale anisotropy in their simulations, which may account for at least part of the difference in the estimates.

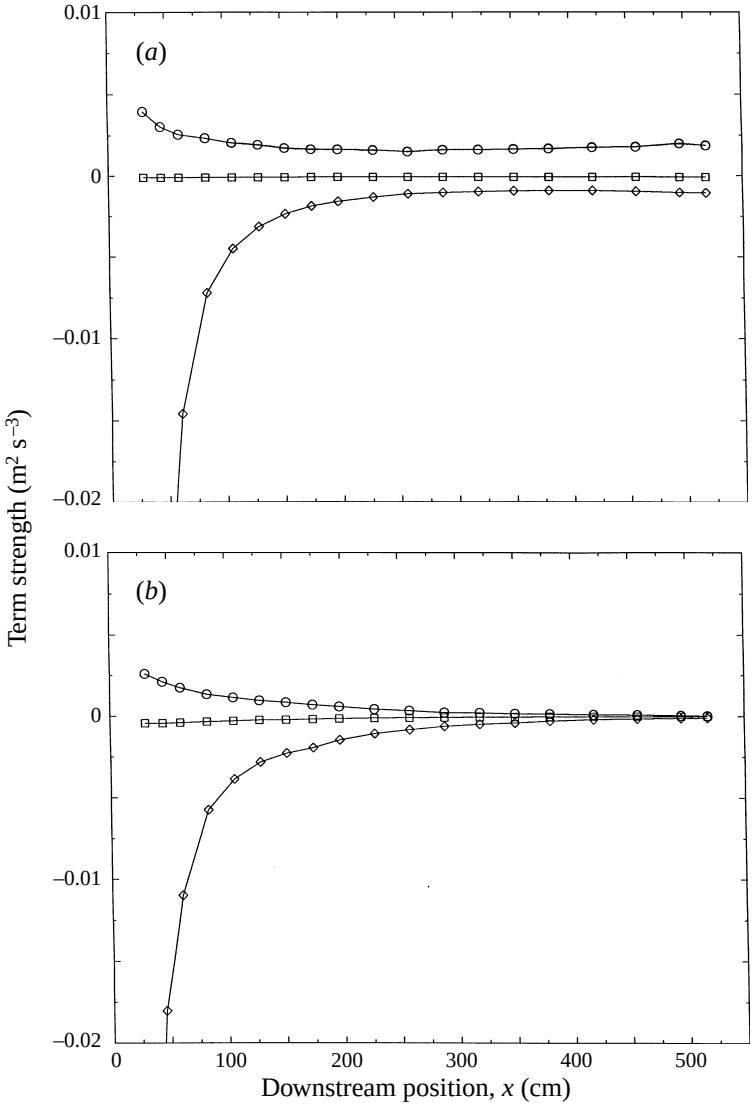

FIGURE 9. Term evolution of turbulent kinetic energy equation: (*a*) 1.45 cm grid, $Ri = 0.04$; (*b*) 0.64 cm grid, $Ri = 0.44$. Symbols: ○---○, production term; □---□, buoyancy term; ◇---◇, dissipation term.

The two terms on the right-hand side of equation (6), the scalar variance equation, are plotted in figure 10 for both of the cases discussed above. In all of these results, we find that the predicted change in θ' is overestimated (i.e. growth rates too high, decay rates too low). This result suggests that we have underestimated the temperature dissipation by amounts of up to 50%. This is in agreement with the experiments of Thoroddsen & Van Atta (1996), who found that the temperature strain rates are highly anisotropic for stably stratified flows, and that using only the longitudinal strain rate will underestimate the dissipation. The simulations of Itsweire *et al.* (1993) also show that using only the streamwise temperature strain may greatly underestimate of χ.

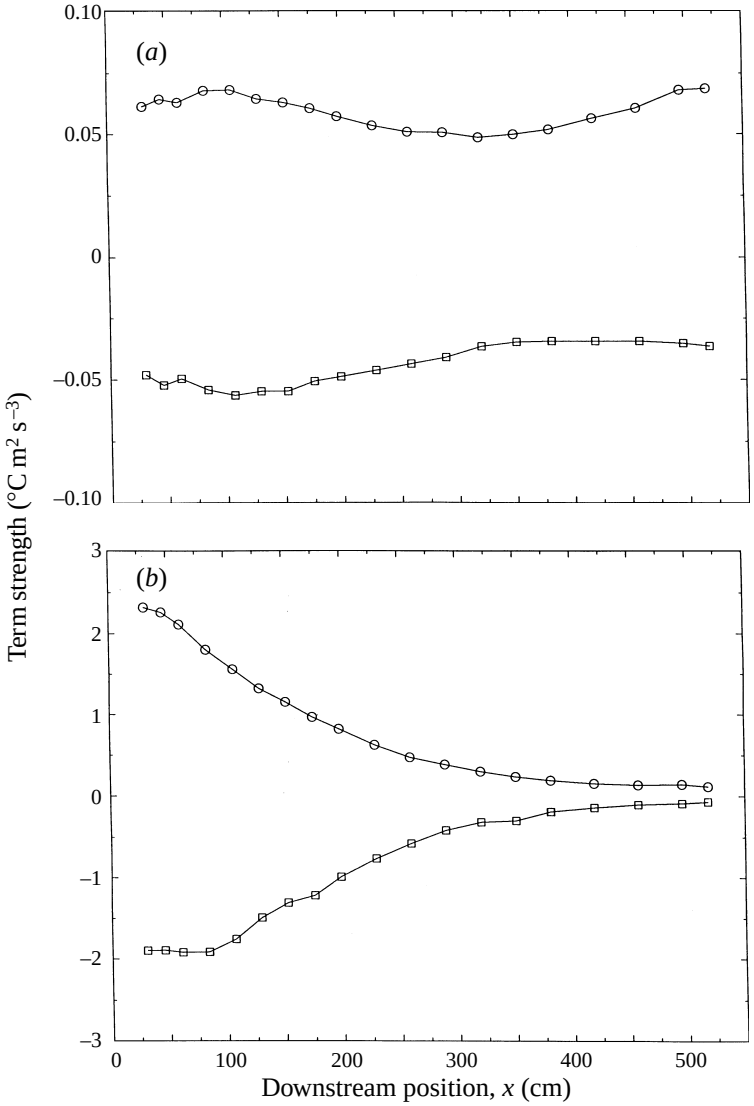

FIGURE 10. Term evolution of scalar variance equation: (*a*) 1.45 cm grid, $Ri = 0.04$; (*b*) 0.64 cm grid, $Ri = 0.44$. Symbols: ○---○, buoyancy term; □---□, dissipation term.

4. Anisotropy in the turbulence

4.1. *Large-scale anisotropy*

In order to study the influence of buoyancy on the anisotropy of the flow at large scales, we first consider the evolution of the ratio w'/u', shown in figure 11(*a*) for the 1.45 cm grid. The results are qualitatively very similar for the different grids. In all cases, w'/u' decreases from a value close to 1.0, the isotropic value, near the grid, to a minimum near 300 cm downstream ($\tau \sim 7.0$); w'/u' then either increases slightly or holds a level value for the remainder of the evolution of the turbulence. Decreasing the mesh size monotonically increases the minimum value of w'/u' from 0.55 for the 5.08 cm grid to 0.38 for the 0.64 cm grid. The evolution of v'/u' is similar to that of w'/u', with two main differences: v'/u' is higher than w'/u', due to the preferential action of the buoyancy term in the w' equation, which acts as a direct sink for w'; and,

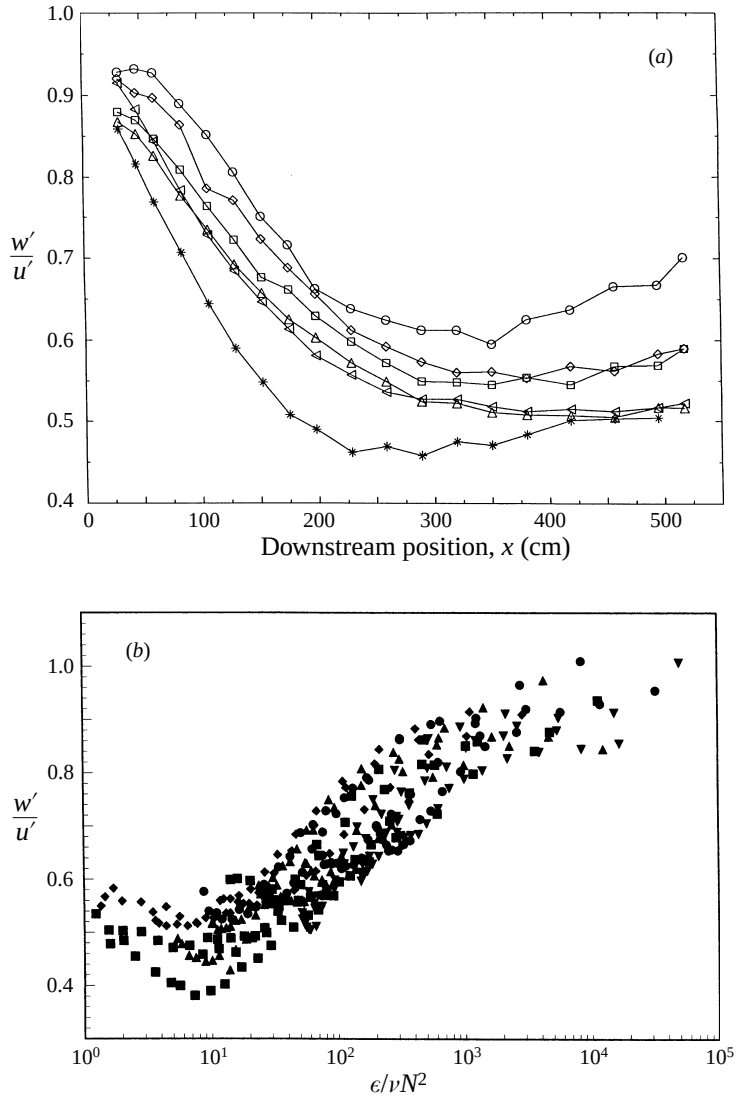

FIGURE 11. Evolution of w'/u' for all Ri, 1.45 cm grid: (a) as a function of downstream position, (b) as a function of $\epsilon/\nu N^2$. Symbols for (a) are the same as in figure 2, and symbols for (b) are: ▼, $Ri = 0.04$; ●, $Ri = 0.08$; ▲, $Ri = 0.12$; ◆, $Ri = 0.19$; ■, $Ri = 0.44$.

v'/u' does not reach a minimum at $\tau = 7$ as does w'/u', but rather continues to decrease throughout the entire run, which extends to about $\tau = 12$. Both the present results and those of Thoroddsen & Van Atta (1992) show that buoyancy affects the r.m.s. lateral velocity about half as much as it does the r.m.s. vertical velocity. The behaviour seen in earlier experiments and simulations is generally qualitatively similar to our results, as discussed in detail by Piccirillo (1993). One exception is that the degree of anisotropy in Gerz *et al.* (1989) does not appreciably increase with increasing Ri, in contrast to the present results.

Comparing our results for $Ri = 0.44$ ($N = 2.23$) to those of Thoroddsen & Van Atta (1992) for $N \sim 2$, we find that the addition of shear decreases w'/u' by about 10% over the unsheared results. Tavoularis & Karnik (1989) summarize all of the previous

research on turbulence in unstratified, uniformly sheared flows to find an asymptotic value for w'/u' of 0.66, which is within the range of our values of 0.77, 0.70, 0.70 and 0.64 for our 5.08 cm, 2.54 cm, 1.45 cm and 0.64 cm grids, respectively, and an asymptotic value of 0.73 for v'/u', as compared with our values of 0.86, 0.80, 0.75 and 0.80.

Yamazaki (1990) has studied the evolution of w'/v' in the ocean thermocline, and he finds significant anisotropy for $\epsilon/\nu N^2 > 200$. The dimensionless parameter $\epsilon/\nu N^2$ (Dillon & Caldwell 1980) is used frequently in the oceanic literature as a primary descriptor of the state of the turbulence (for example, by Gibson 1980). There is some disagreement as to the possible physical significance of this quantity, as Gargett, Osborn & Nasmyth (1984) have referred to it as a buoyancy-based Reynolds number, while other researchers (for example, Gregg 1987) have referred to it as a Froude number. To compare with Yamazaki's results, our data for w'/u' are plotted against $\epsilon/\nu N^2$ in figure 11(*b*). Our results show that for $\epsilon/\nu N^2$ of up to at least 2000 there remains a significant level of anisotropy in the flow, as in Yamazaki's thermocline data. This suggests caution in using isotropic formulae for $\epsilon/\nu N^2 < 2000$. Indeed, Gargett *et al.* (1984) find that their ocean spectra do show deviations from isotropic behaviour for $\epsilon/\nu N^2 < 2000$, although the inertial scales are roughly isotropic for $\epsilon/\nu N^2 > 200$.

4.2. *Small-scale anisotropy*

One measure of small-scale anisotropy in the flow is how much the values of the ratios of different r.m.s. strain rates differ from what their values would be for isotropic turbulence. The ratio of the r.m.s. horizontal gradients of the vertical and streamwise velocity fluctuations, S_{wu}, is

$$S_{wu} = \frac{\overline{(\partial w/\partial x)^2}}{\overline{(\partial u/\partial x)^2}}. \tag{9}$$

S_{wu} is shown in figure 12(*a*) for the 1.45 cm grid. The results are remarkably uniform for each of the grids, with S_{wu} decreasing from a value of close to 2 (the isotropic value) near the grid to a minimum at $x = 250$–300 cm downstream ($\tau = 5.5$–7.0), whereupon it levels out, or, if the turbulent kinetic energy is growing, it increases back towards a value of 2.0. S_{wu} is a decreasing function of Ri, and it is an increasing function of the grid mesh size. The amount of anisotropy is very large. For example, for $Ri = 0.44$, for the 1.45 cm grid, $S_{wu} < 0.25$, a value less than 1/8 of the isotropic value. The anisotropy is numerically greater than for the variance $(w'/u')^2$. For unsheared, non-stratified, decaying turbulence, Thoroddsen & Van Atta (1992) found that the value of S_{wu} remains near 2.0. For the present unstratified ($Ri = 0$) data, one sees that the anisotropy induced by the mean shear alone is large, and while the turbulence is still decaying, becomes about 2/3 as large as the maximum anisotropy produced by the combined effects of shear and stratification. The robust increase back toward the isotropic value of 2.0 as the turbulence grows for $Ri = 0$, and a similar, weaker, trend for small values of Ri, may be interpreted as an expected consequence of the increasing value of the Reynolds number in the downstream direction in those cases. The clear effect of buoyancy in enhancing small-scale anisotropy contradicts the traditional picture of buoyancy as a force which primarily affects that largest scales of turbulence. In fact, in a relative sense, buoyancy has more effect on the small scales of the flow.

Similar behaviour was found in the evolution of S_{vu}, defined as

$$S_{vu} = \frac{\overline{(\partial v/\partial x)^2}}{\overline{(\partial u/\partial x)^2}}. \tag{10}$$

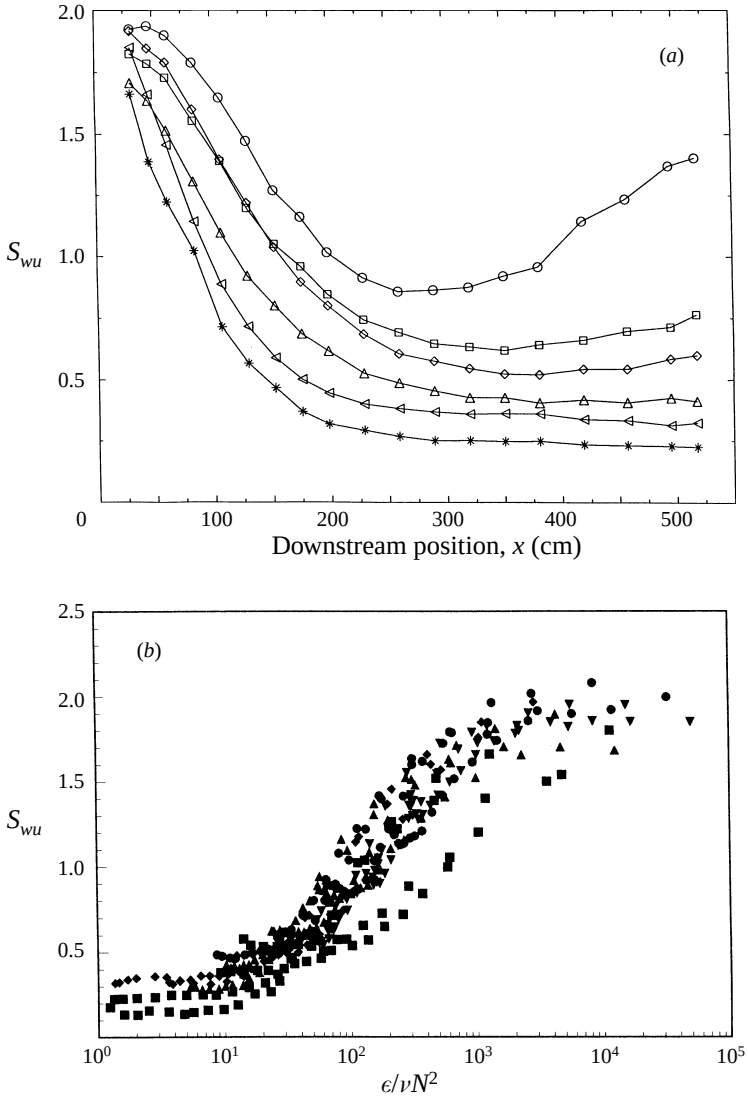

FIGURE 12. Evolution of $S_{wu} = \overline{(\partial w/\partial x)^2}/\overline{(\partial u/\partial x)^2}$ for all Ri, 1.45 cm grid: (*a*) as a function of downstream position, (*b*) as a function of $\epsilon/\nu N^2$. Symbols are the same as in figure 11.

As in the case of S_{wu}, anisotropy increases with Ri, from S_{vu} values close to 2 for $Ri = 0$ to values between 0.50 and 0.75 for $Ri = 0.44$ at $\tau = 12$ (compared with values between 0.23 and 0.50 for S_{wu}). S_{vu} continues to decline throughout the entire length of the test section, in contrast to S_{wu}, which reaches a minimum and then levels off. For their unsheared flow, Thoroddsen & Van Atta (1996) report a minimum value for S_{vu} of 0.75 for $N = 3.03$ rad s^{-1}.

Rohr *et al.* (1988*b*) do not report any strain-rate data. The simulation data of Holt *et al.* (1992) has been used by Itsweire *et al.* (1993) to estimate all nine strain rates:

$$s_{ij} = \overline{\left(\frac{\partial u_i}{\partial x_j}\right)^2}, \tag{11}$$

which are needed to measure the dissipation. Unfortunately, as mentioned earlier, for

these DNS and those of Gerz *et al.*, the small scales are initially very anisotropic, hindering comparison with our experiments, for which the small scales are initially nearly isotropic. For example, in the Holt *et al.* results, S_{wu} is much less than the isotropic value of 2 for all of the Ri shown, with a minimum value of 0.5 reached at $Ri = 0.37$, higher than our result of 0.37 for the 5.08 cm grid with $Ri = 0.44$. Their $Ri = 0$ case has an S_{wu} of 1.0, much lower than our value of 1.5–1.7 for the 5.08 cm grid case.

Gargett *et al.* (1984) suggest that for $\epsilon/\nu N^2 > 200$, only one strain rate is needed to compute the viscous dissipation. To test this result, we plotted S_{wu} against $\epsilon/\nu N^2$, as shown in figure 12(*b*). In our w'/u' results, for $\epsilon/\nu N^2 < 2000$, there is a significant amount of anisotropy in our data, which precludes using only one strain rate to calculate the dissipation. Yamazaki & Osborn (1990), using thermocline data, find significant anisotropy for S_{wv} when $\epsilon/\nu N^2 < 100$. However, given our S_{wu} and S_{vu} results, it seems likely that S_{wv} is not a good measure of anisotropy, as both S_{wu} and S_{vu} could decrease in such a way as to obscure the anisotropy in the strain rates. It seems a safe proposition that for $\epsilon/\nu N^2 < 2000$, stratified turbulence is not isotropic, and assuming it to be so could lead to serious errors.

5. Spectral evolution of the turbulence

5.1. *Power spectra*

Figure 13 shows representative plots of the evolution of the u-component power spectrum $E_{uu}(f)$. Initially, for all Ri studied, $E_{uu}(f)$ decays at all frequencies. This situation persists to $x \sim 150$ ($\tau \sim 3.5$), when the large-scale (small-frequency) energy begins to grow, while the small-scale energy continues to decay. In this mixed evolution, shown in figure 13(*a*) for $Ri = 0$, and in figure 13(*b*) for $Ri = 0.19$, the frequency at which the spectra remain constant, f_c, does not change as the flow evolves downstream. This suggests that the shear forces and the dissipative forces each have very distinct scales of control in the flow, and that when the shear dominates the dissipative region, it dominates it as a whole, not piecemeal.

For $Ri = 0$, there is another transition in the spectral behaviour, at $\tau = 7$, between mixed evolution, and evolution where the spectra are growing at all scales, shown in figure 13(*c*). This transition always occurs in the same way: energy at frequencies higher than f_c stops decreasing and begins to increase as a unit. When $0 < Ri < Ri_{cr}$, the mixed evolution behaviour in $E_{uu}(f)$ persists throughout the test section. When $Ri > Ri_{cr}$, the mixed evolution behaviour is slightly modified, in that the large-scale energy is very nearly constant, while the small-scale energy decreases.

The behaviour of $E_{ww}(f)$ and $E_{vv}(f)$ is almost exactly the same, for all Ri, as $E_{uu}(f)$. The only qualitative difference is that for $Ri > Ri_{cr}$ the $E_{ww}(f)$ spectra increase at large scales while decaying at small scales, in contrast to $E_{uu}(f)$, where the large-scale spectra are constant. Quantitatively, the frequency f_c is not same for the three power spectra. However, no clear pattern in the value of f_c could be found.

Rohr *et al.* (1988*b*) also found for $Ri > Ri_{cr}$ that the small-scale energy is decaying while the large-scale energy is constant. They interpret this as showing the creation of internal waves in the flow, and they use a Kolmogorov scaling to argue that the mean shear's affect on the flow at this Ri is small. However, from our strong evidence that the large scales in our flow are continuing to actively mix (see §5.2), it appears that for our flow the mean shear is still creating energy at the large scales.

The spectra of Holt *et al.* (1992) show some significant differences when compared to our results. For $E_{uu}(f)$, Holt *et al.* find a similar mixed behaviour to ours for $Ri <$

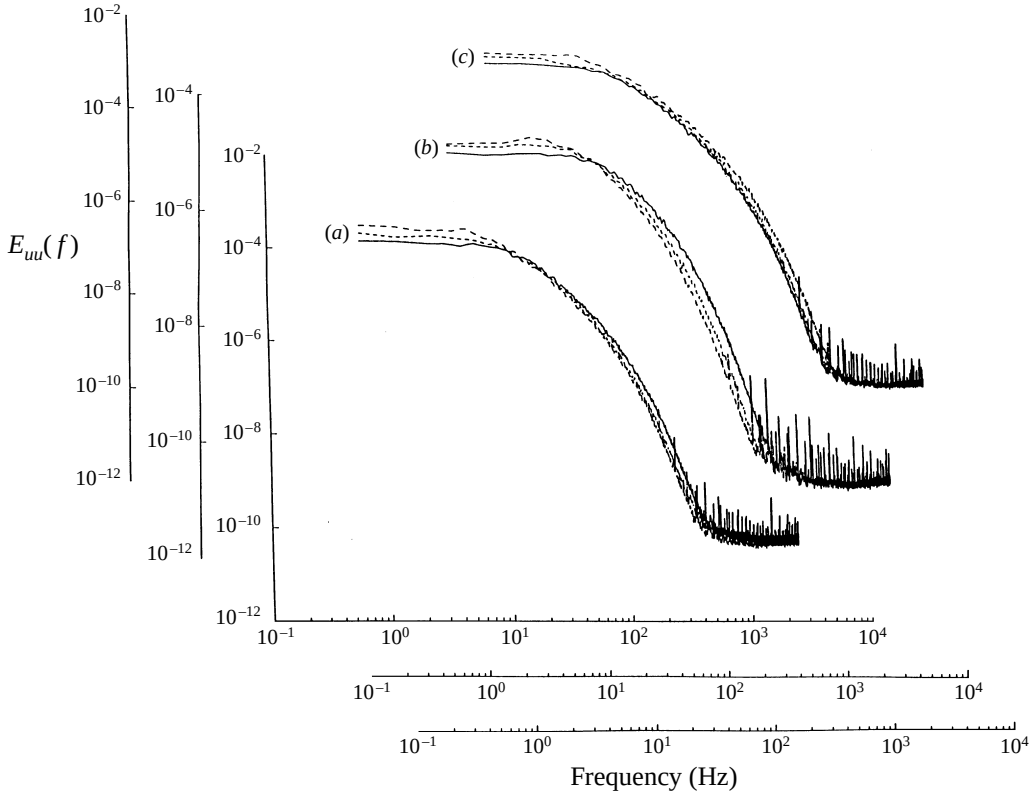

FIGURE 13. Evolution of $E_{uu}(f)$, showing the two types of spectral evolution seen in all the results. (*a*) Initial evolution of $E_{uu}(f)$ for the 2.54 cm grid, with $Ri = 0$. Symbols: ——, $x = 175.3$ cm; ----, $x = 228.6$ cm; – – –, $x = 320.0$ cm. (*b*) Final evolution of $E_{uu}(f)$, 1.45 cm grid, with $Ri = 0.19$. Symbols: ——, $x = 320$ cm; ----, $x = 419.1$ cm; – – –, $x = 495.3$ cm. (*c*) Final evolution of $E_{uu}(f)$ for the 2.54 cm grid, with $Ri = 0$. Symbols: ——, $x = 350.5$ cm; ----, $x = 419.1$ cm; – – –, $x = 495.3$ cm. Both (*a*) and (*b*) show mixed spectral evolution, where the spectrum increases at low wavenumbers and decreases at high wavenumbers, while (*c*) shows spectral evolution where the spectrum is increasing at all wavenumbers.

Ri_{cr}. When $Ri > Ri_{cr}$, the frequency f_c changes as the flow evolves, unlike in our results. For $E_{ww}(f)$, at all Ri reported, the frequency f_c again changes as the flow evolves. Gerz *et al.* (1989) do not report on spectral evolution.

Holt *et al.* (1992) have estimated the nonlinear streamwise energy transfer $N_{uu}(f)$ (defined in Holt 1990) as a function of Ri, and found that as Ri increases, $N_{uu}(f)$ decreases. This result suggests that at sufficiently high Ri, the turbulence will have the mixed spectral evolution found in both our results and Holt *et al.*'s, in which the large scales increase in energy while the small scales decrease in energy. This is because with decreased energy transfer, energy will not be able to move from large to small scales to offset the small-scale energy lost to dissipation. Thus, the small scales will be destroyed by viscous forces while the large scales continue to grow due to the mean shear.

Suppression of spectral energy transfer occurs through the same mechanism by which buoyancy affects non-sheared flows: suppression of overturns. However, in the case of sheared flows, a sufficiently large mean shear can dominate the behaviour of the largest scales of the flow, with buoyancy dominating at smaller scales. The resultant

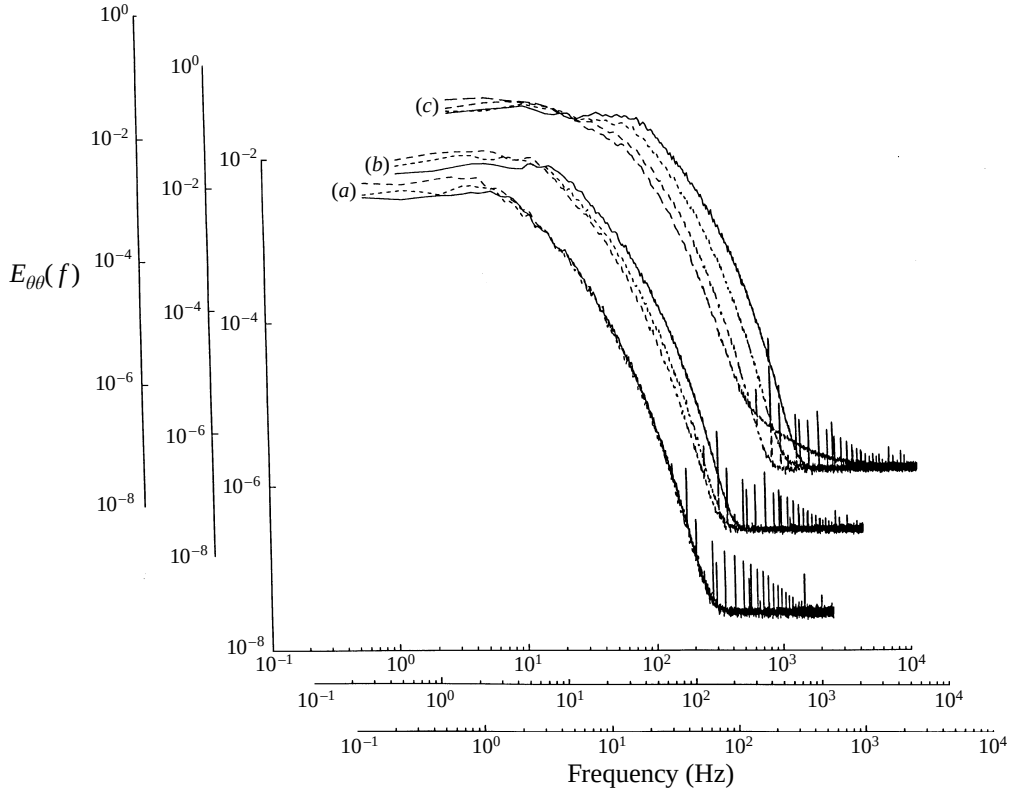

FIGURE 14. Final evolution of $E_{\theta\theta}(f)$, for (*a*) 2.54 cm grid, with $Ri = 0.04$; (*b*) 1.45 cm grid, with $Ri = 0.19$; and (*c*) 0.64 cm grid, with $Ri = 0.44$. Symbols for all are the same as in figure 13(*b*). (*a*) Shows spectral evolution where the spectrum is increasing at low wavenumbers and stationary at high wavenumbers, while (*b*) and (*c*) show mixed spectral evolution.

suppression of overturns in this energy range results in a reduction of the cascade of energy transfer to smaller scales.

Since the suppression of spectral energy transfer by buoyancy forces is done preferentially, the transfer of vertical velocity turbulent energy (w') will be more inhibited by buoyancy forces than the transfer of lateral- or streamwise-velocity turbulent energy (v' and u'). One might expect the small scales in the flow to reflect this anisotropic transfer. While this preferential suppression of energy transfer may be responsible for the large degree of small-scale anisotropy, anisotropy at small scales could alternatively be created directly by buoyancy forces, as suggested by Thoroddsen & Van Atta (1992).

The evolution of the temperature spectrum $E_{\theta\theta}(f)$ for the 2.54 cm grid runs is shown in figure 14, for $Ri = 0.04$, 0.19 and 0.44. As with the velocity spectra, the evolution of the temperature spectra is clearly of the mixed type. When $Ri < Ri_{cr}$, the spectra evolve through the mixed evolution described above, where the spectra are increasing at the large scales and decreasing at the small scales, to a different mixed evolution, where the spectra are increasing at large scales and roughly constant at small scales (figure 14*a*). When $Ri = Ri_{cr}$ (figure 14*b*), the mixed evolution seen for the velocity spectra persists throughout the test section, with one difference: the frequency f_c is continually shifting to lower frequencies (bigger scales), starting out at around 30 Hz at $\tau = 1$ and ending up at around 5 Hz at $\tau = 12$. This suggests that eventually θ' must decrease, as there

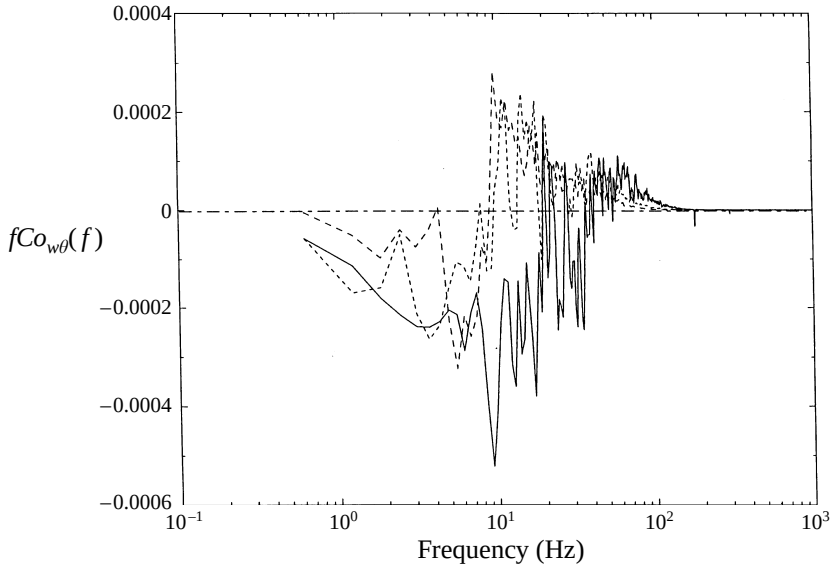

FIGURE 15. Evolution of $fCo_{w\theta}(f)$, 2.54 cm grid, $Ri = 0.44$. Symbols same as in figure 13(*b*).

will be no scales remaining that are able to increase their energy. Note that the velocity and temperature spectra, which are Fourier transforms of two-point second-order correlations, continuously evolve even for $Ri = Ri_{cr}$, after the single-point second-order moments have become constant. For $Ri > Ri_{cr}$ (figure 14*c*), the spectra show the mixed evolution seen for $Ri = Ri_{cr}$, but now the large-scale energy is increasing very slowly, and is overwhelmed by the energy decrease at small scales. The results of Rohr *et al.* (1988*b*) are qualitatively identical to our results, while Holt *et al.* and Gerz *et al.* do not report temperature spectral results.

5.2. *Buoyancy-flux cospectral evolution*

For the $Ri = 0.44$ case, we find $0 < R_{w\theta} < 0.10$, indicating that while there is no net flux reversal, it is possible that for some range of frequencies there may be a local flux reversal. Figure 15 shows three cospectral plots in area-preserving coordinates for $Ri = 0.44$. A negative value of $Co_{w\theta}(f) = \mathrm{Re}[E_{w\theta}(f)]$ signifies downgradient flux, while a positive value signifies countergradient flux. In the region from 10 Hz to 100 Hz (corresponding to scales of 3 cm down to 3 mm) $Co_{w\theta}(f) > 0$ and thus the flow is restratifying by countergradient buoyancy flux at these small scales. Similar behaviour for large Ri and $Pr = 1$ was seen in the simulation of Holt *et al.* (1992). The present experiments thus verify the physical reality of one of the most interesting predictions of the simulations. Gerz *et al.* also find small-scale flux reversal, although only at higher Prandtl number. The presence of shear has a dramatic effect on the behaviour of the buoyancy flux, in that now flux reversals, which occurred at the largest scales of the unsheared flow (Lienhard & Van Atta 1990), are now occurring at small scales. The results of Rohr *et al.* are not conclusive in this region because of the large wavenumber bin size necessary in the reduction of their data.

An important use of $Co_{w\theta}(f)$ is as a diagnostic tool for assessing the presence of linear internal waves. As discussed by Stewart (1969), if the phase angle ϕ between the w- and θ-fluctuations, where $\phi = -Qu_{w\theta}(f)/Co_{w\theta}(f)$, is 180°, then the flux is downgradient, while $\phi = 0°$ implies restratification, and $\phi = 90°$ shows the presence of linear

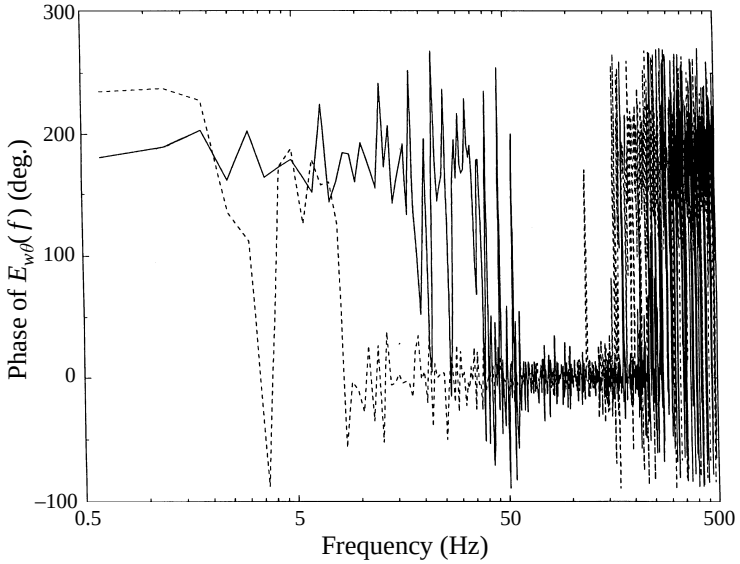

FIGURE 16. Phase evolution of $E_{w\theta}(f)$, 1.45 cm grid, $Ri = 0.44$. Symbols same as in figure 13(*b*).

internal waves. In figure 16, we show two phase-angle plots, for two of the data sets shown in figure 15. There is clearly evidence of large-scale downgradient flux, where ϕ is 180°, and of small-scale restratification, where ϕ is 0° ($Qu_{w\theta}(f) = \mathrm{Im}[E_{w\theta}(f)]$). We see no indication in any of our results of phase-angle behaviour characteristic of linear internal wave activity. The restratification is moving to larger scales as the flow evolves, which suggests that buoyancy effects are being felt by the turbulence at larger scales as the flow evolves. In all our results, however, we clearly see that the largest scales of the flow are producing downgradient flux. The Reynolds stress cospectrum $Co_{uw}(f) = \mathrm{Re}[E_{uw}(f)]$ was also investigated. Our results showed that for all Ri, $Co_{uw}(f)$ remained positive at large scales, indicating that even at high Ri, the mean shear is creating energy in the flow at the largest scales.

6. Conclusions

The value of the critical Richardson number Ri_{cr} for a stably stratified homogeneous shear flow was found to be a strongly increasing function of the shear parameter Sq^2/ϵ, in agreement with the behaviour found for small initial values of Sq^2 in numerical simulations by Jacobitz *et al.* (1994, 1996). For sufficiently small values of the shear number, Ri_{cr} takes values an order of magnitude lower than the critical value of 1/4 obtained by Miles (1961) and Howard (1961) as an upper bound for growth for disturbances via linearized stability analysis or stably stratified laminar flow. This strong dependence of Ri_{cr} on Sq^2/ϵ suggests that the shear number may also play an important role in more complex stably stratified turbulent shear flows, such as those occurring in the atmosphere and oceans, and should be taken into account when attempting to correlate turbulent stirring and resultant mixing with values of Ri.

The large scales of the flow evolved from an initial nearly isotropic state to a very anisotropic one. The degree of anisotropy increased with increasing Richardson number Ri. The persistent small-scale anisotropy for $Ri > Ri_{cr}$ is similar to that found by Thoroddsen & Van Atta (1992) for unsheared decaying stably stratified turbulence. For $Ri = 0$, the small scales robustly returned toward a state of local isotropy as the

turbulent kinetic energy grew, and a similar, but much weaker, trend was observed for stratified flows with $Ri < Ri_{cr}$. The mixed evolution of the velocity power spectra, where the energy at large scales increased while the energy at small scales decreased, suggests that the anisotropy at the small scales is caused by buoyancy forces reducing spectral transfer to these scales. For sufficiently large Ri countergradient heat flux occurred at small scales, as found in the earlier simulations of Gerz *et al*. (1989) and Holt *et al*. (1992).

This study was funded by the Office of Naval Research, Small Scale Physical Oceanography contract number N00014-94-1-0233, and the National Science Foundation, Physical Oceanography Grant number OCE 92-17213. Many helpful discussions have occurred over the course of this research, most usefully with Professor Jeffrey Koseff of Stanford University, Professor Fred Browand of the University of Southern California, Dr Ken Helland of Data Ready Corporation, and Professor Sigurdur Thoroddsen of the University of Illinois at Urbana-Champagne.

REFERENCES

Barrett, T. J. & Van Atta, C. W. 1989 Experiments on the inhibition of mixing in stably stratified decaying turbulence using laser Doppler anemometry and laser-induced turbulence. *Phys. Fluids* A **3**, 1321–1332.

Britter, R. E. 1988 Laboratory experiments on turbulence in density-stratified fluids. *Proc. 8th AMS-Conf. on Turbulence and Diffusion, April 26–29, 1988, San Diego*.

Budwig, R., Tavoularis, S. & Corrsin, S. 1985 Temperature fluctuations and heat flux in grid-generated isotropic turbulence with streamwise and transverse mean-temperature gradients. *J. Fluid Mech.* **153**, 441–460.

Champagne, F. H., Harris, V. G. & Corrsin, S. 1970 Experiments on nearly homogeneous shear flow. *J. Fluid Mech.* **41**, 81–139.

Dillon, T. M. & Caldwell, D. R. 1980 The Batchelor spectrum and dissipation in the upper ocean. *J. Geophys. Res.* **85**, 1910–1916.

Feiereisen, W. J., Shirani, E., Ferziger, J. H. & Reynolds, W. C. 1982 Direct simulation of homogeneous shear flow on Illiac IV computer: Applications to compressible and incompressible modeling. In *Turbulent Shear Flows 3* (ed. J. S. Bradbury, F. Durst, B. E. Launder, F. W. Schmidt & J. H. Whitelaw) p. 309. Springer.

Fincham, A. M., Maxworthy, T. & Spedding, G. R. 1997 The horizontal and vertical structure of the vorticity field in freely-decaying, stratified grid-turbulence. *Dyn. Atmos. Oceans*, in press.

Gargett, A. E., Osborn, T. R. & Nasmyth, P. W. 1984 Local isotropy and the decay of turbulence in a stratified fluid. *J. Fluid Mech.* **144**, 231–280.

Gerz, T. & Schumann, U. 1991 Direct simulation of homogeneous turbulence and gravity waves in sheared and unsheared stratified flows. In *Turbulent Shear Flows* (ed. W. C. Reynolds) pp. 27–45. Springer.

Gerz, T., Schumann, U. & Elghobashi, S. E. 1989 Direct numerical simulation of stratified homogeneous turbulent shear flows. *J. Fluid Mech.* **200**, 563–594.

Gibson, C. H. 1980 Fossil temperature, salinity, and vorticity turbulence in the ocean. In *Marine Turbulence* (ed. J. C. T. Nihoul), pp. 221–257. Elsevier.

Gregg, M. C. 1987 Diapycnal mixing in the thermocline: A review. *J. Geophys. Res.* **92**, 5249–5286.

Harris, V. G., Graham, J. A. & Corrsin, S. 1977 Further experiments in nearly homogeneous turbulent shear flow. *J. Fluid Mech.* **81**, 657–687.

Herring, J. R. & Metais, O. 1989 Numerical experiments in forced stably stratified flow. *J. Fluid Mech.* **202**, 97–115.

Holt, S. E. 1990 The evolution and structure of homogeneous stably stratified sheared turbulence. PhD thesis, Stanford University.

Holt, S. E., Koseff, J. R. & Ferziger, J. H. 1992 A numerical study of the evolution and structure of homogeneous stably stratified sheared turbulence. *J. Fluid Mech.* **237**, 499–539.

HOWARD, L. N. 1961 Note on a paper of John Miles. *J. Fluid Mech.* **10**, 509–512.

HUNT, J. C. R., STRETCH, D. D. & BRITTER, R. E. 1988 Length scales in stably stratified turbulence and their use in turbulence models. In *Stably Stratified Flows and Dense Gas Dispersions* (ed. J. S. Puttock), pp. 285–321. Clarendon.

ITSWEIRE, E. C., HELLAND, K. N. & VAN ATTA, C. W. 1986 The evolution of grid generated turbulence in a stably stratified fluid. *J. Fluid Mech.* **162**, 299–338.

ITSWEIRE, E. C., KOSEFF, J. R., BRIGGS, D. A. & FERZIGER, J. H. 1993 Turbulence in stratified shear flows: Implications for interpreting shear-induced mixing in the ocean. *J. Phys. Oceanogr.* **23**, 1508–1522.

IVEY, G. N. & IMBERGER, J. 1991 On the nature of turbulence in a stratified fluid, Part 1: The energetics of mixing. *J. Phys. Oceanogr.* **21**, 650–658.

IVEY, G. N., KOSEFF, J. R., BRIGGS, D. A. & FERZIGER, J. H. 1992 Mixing in a stratified shear flow: energetics and sampling. *CTR Ann. Res. Briefs*, pp. 335–344.

JACOBITZ, F., SARKAR, S. & VAN ATTA, C. W. 1994 Direct numerical simulation of a stratified turbulent shear flow. Abstract in *Bull. Am. Phys. Soc.* **39**, 1914.

JACOBITZ, F., SARKAR, S. & VAN ATTA, C. W. 1996 Direct numerical simulation of a stratified turbulent shear flow. *J. Fluid Mech.* (submitted).

KALTENBACH, H. J., GERZ, T. & SCHUMANN, U. 1994 Large-eddy simulation of homogeneous turbulence and diffusion in stably stratified shear flow. *J. Fluid Mech.* **280**, 1–40.

KOMORI, S., UEDA, H., OGINO, F. & MIZUSHINA, T. 1983 Turbulence structure in stably stratified open-channel flow. *J. Fluid Mech.* **130**, 13–26.

LIENHARD, J. H. 1988 The decay of turbulence in thermally stratified flow. PhD thesis, University of California, San Diego.

LIENHARD, J. H. & VAN ATTA, C. W. 1990 The decay of turbulence in thermally stratified flow. *J. Fluid Mech.* **210**, 57–112.

LIU, H.-T. 1995 Energetics of grid turbulence in a stably stratified fluid. *J. Fluid Mech.* **269**, 127–157.

MILES, J. W. 1961 On the stability of heterogeneous shear flows. *J. Fluid Mech.* **10**, 496–508.

PICCIRILLO, P. 1993 An experimental study of the evolution of turbulence in a uniformly sheared thermally stratified flow. PhD thesis, University of California, San Diego.

PICCIRILLO, P. & VAN ATTA, C. W. 1996. A new wind tunnel for producing arbitrary vertical temperature and velocity profiles. *Exps. Fluids* **21**, 66–69.

RILEY, J. J., METCALFE, R. W. & WEISSMAN, M. A. 1981 Direct numerical simulations of homogeneous turbulence in density stratified fluids. In *Nonlinear Properties of Internal Waves* (ed. B. J. West). AIP Conf. Proc. vol. 76.

ROGALLO, R. S. 1981 Numerical experiments in homogeneous turbulence. *NASA Tech. Mem.* 81315.

ROGALLO, R. S. & MOIN, P. 1984 Numerical simulation of turbulent flows. *Ann. Rev. Fluid Mech.* **16**, 99–137.

ROGERS, M. M., MOIN, P. & REYNOLDS, W. C. 1986 The structure and modeling of the hydrodynamic and passive scalar fields in homogeneous turbulent flows. *Dept. Mech. Engng Rep.* TF-25, Stanford University.

ROHR, J. J. 1985 An experimental study of evolving turbulence in uniform mean shear flows with and without stable stratification. PhD thesis, University of California, San Diego.

ROHR, J. J., ITSWEIRE, E. C., HELLAND, K. N. & VAN ATTA, C. W. 1988*a* An investigation of the growth of turbulence in a uniform mean shear flow. *J. Fluid Mech.* **187**, 1–33.

ROHR, J. J., ITSWEIRE, E. C., HELLAND, K. N. & VAN ATTA, C. W. 1988*b* Growth and decay of turbulence in a stably stratified shear flow. *J. Fluid Mech.* **195**, 77–111.

ROSE, W. G. 1966 Results of an attempt to generate a homogeneous turbulent shear flow. *J. Fluid Mech.* **25**, 97–120.

ROSE, W. G. 1970 Interaction of grid turbulence with a uniform mean shear. *J. Fluid Mech.* **44**, 767–779.

SCHUMANN, U. & GERZ, T. 1995 Turbulent mixing in stably stratified shear flows. *J. Appl. Met.* **34**, 33–48.

SINGH KHALSA, S. S. & GREENHUT, G. K. 1987 Convective elements in the marine atmospheric boundary layer II: Entrainment at the capping inversion. *J. Clim. Appl. Met.* **26**, 824–836.

STEWART, R. W. 1969 Turbulence and waves in a stratified atmosphere. *Radio Sci.* **4**, 1269–1278.

STILLINGER, D. C., HELLAND, K. N. & VAN ATTA, C. W. 1983 Experiments on the transition of homogeneous turbulence to internal waves in a stratified fluid. *J. Fluid Mech.* **131**, 91–122.

TAVOULARIS, S. & CORRSIN, S. 1981*a* Experiments in a nearly homogeneous shear flow with uniform mean temperature gradient. Part 1. *J. Fluid Mech.* **104**, 311–347.

TAVOULARIS, S. & CORRSIN, S. 1981*b* Experiments in a nearly homogeneous shear flow with uniform mean temperature gradient. Part 2. The fine structure. *J. Fluid Mech.* **104**, 349–367.

TAVOULARIS, S. & KARNIK, U. 1989 Further experiments on the evolution of turbulent stresses and scales in uniformly sheared turbulence. *J. Fluid Mech.* **204**, 457–478.

TENNEKES, H. & LUMLEY, J. L. 1972 *A First Course in Turbulence*. MIT Press.

THORODDSEN, S. T. 1991 Experiments on the statistical nature of stably stratified turbulence. PhD thesis, University of California, San Diego.

THORODDSEN, S. T. & VAN ATTA, C. W. 1992 The influence of stable stratification on small-scale anisotropy and dissipation in turbulence. *J. Geophys. Res.* **97**, 3647–3658.

THORODDSEN, S. T. & VAN ATTA, C. W. 1996 Experiments on density-gradient anisotropies and scalar dissipation of turbulence in stably stratified fluid. *J. Fluid Mech.* **322**, 383–409.

TURNER, J. S. 1973 *Buoyancy Effects in Fluids*. Cambridge University Press.

WEBSTER, C. A. G. 1964 An experimental study of turbulence in a density-stratified shear flow. *J. Fluid Mech.* **19**, 221–245.

YAMAZAKI, H. 1990 Stratified turbulence near a critical dissipation rate. *J. Phys. Oceanogr.* **20**, 1583–1598.

YAMAZAKI, H. & OSBORN, T. 1990 Dissipation estimates for stratified turbulence. *J. Geophys. Res.* **95**, 9739–9744.

YAP, C. T. & VAN ATTA, C. W. 1993 Experimental studies of the development of quasi-two-dimensional turbulence is stably stratified fluid. *Dyn. Atmos. Oceans* **19**, 289–323.

YOON, K. & WARHAFT, Z. 1990 The evolution of grid generated turbulence under conditions of stable thermal stratification. *J. Fluid Mech.* **215**, 601–638.